Computers and Structures 132 (2014) 99–112

Contents lists available at ScienceDirect

Computers and Structures

journal homepage: www.elsevier.com/locate/compstruc

The solution of Maxwell's equations in multiphysics

Klaus-Jürgen Bathe [a,*], Hou Zhang [b], Yiguang Yan [b]

[a] Massachusetts Institute of Technology, Cambridge, MA, USA
[b] ADINA R&D, Inc., Watertown, MA, USA

ARTICLE INFO

Article history:
Received 20 August 2013
Accepted 29 September 2013
Available online 19 November 2013

Keywords:
Electromagnetics
Maxwell's equations
Structures
Navier–Stokes equations
Multiphysics
Fully-coupled response

ABSTRACT

We consider the solution of the fully-coupled equations of electromagnetics with fluid flows and structures. The electromagnetic effects are governed by the general Maxwell's equations, the fluid flows by the Navier–Stokes equations, and the solids and structures by the general Cauchy equations of motion. We present an effective general finite element formulation for the solution of the Maxwell's equations and demonstrate the coupling to the equations for fluids and structures. For the solution, we can use the electric field and magnetic field intensities, or the electric and magnetic potentials, with advantages depending on the problem solved. We give various example solutions that illustrate the use of the solution procedure.

1. Introduction

During the recent years, an increasing emphasis has been placed on the solution of multiphysics problems [1]. While the solution of problems considered separately in solids and structures, in fluid flows, and in electromagnetics (EM) has been pursued for decades – and widely-used quite powerful computer programs are now available – the solution of problems in which general structures interact with fluid flows and electromagnetic waves has hardly been tackled and presents special difficulties. Indeed, only specific problems have been solved in which the solution techniques have been developed specifically for the physical problem considered, see for example, refs. [2–11].

Considering the analysis of solids and structures coupled with fluid flows, many publications have recently appeared, and numerous applications are found, in particular, in biomechanics and the automotive and airplane industries. The next step for general multiphysics solutions is clearly that electromagnetic effects should also be included. In today's time, electrical devices are used daily by almost everybody in a multitude of applications, and to reach optimal designs the structural, fluid and electromagnetic fully-coupled effects would ideally be considered. These coupled effects can be particular important, for example, in problems of magneto-solid and fluid mechanics, in medical applications and biomedical engineering, metal processing, and plasma physics, see ref. [12] and the references therein.

Numerous publications are also available on the numerical solution of electromagnetic field problems. In the most general cases, the general Maxwell's equations are considered. However, while finite element solutions have been obtained for some decades, the earliest attempts frequently showed spurious modes and in that sense were not reliable [13,14]. Thereafter, special finite element schemes were designed, and in particular the edge-based elements [15]. These elements are more reliable but have the shortcomings that the edge degrees of freedom are difficult to couple with the usual nodal degrees of freedom used in the finite element analyses of fluid flows and structures, divergence-free conditions are considered, the convergence is not optimal, and the elements do not directly fit into the usual post-processing schemes used. In more recent research, various discontinuous finite element schemes and meshless methods have been proposed, see for example, Nicomedes et al. [16] and Badia and Codina [17], but these procedures are computationally quite costly or contain artificial numerical factors for general practical analyses.

Our objective in this paper is to present a novel finite element scheme for the solution of the general Maxwell's equations specifically developed to solve for electromagnetic effects coupled with fluid flows, solids and structures, while keeping our philosophy for the development of finite element procedures in mind [18]. Since we amply published on our solution procedures for fluid flows with structural interactions previously [19–22], we focus in this paper on the solution of Maxwell's equations, to couple with the governing equations of fluids and structures. We consider the static and harmonic solutions of the Maxwell's equations, including the solution of high-frequency problems, and present a general uniform procedure for solution in which either the primitive

* Corresponding author. Tel.: +1 6179265199.
E-mail address: kjb@mit.edu (K.J. Bathe).

0045-7949/$ - see front matter © 2013 Elsevier Ltd. All rights reserved.
http://dx.doi.org/10.1016/j.compstruc.2013.09.006

variables of electric and magnetic fields are used (**E** and **H**), or the scalar electric and vector magnetic potentials (ϕ and **A**) are employed. The finite elements used are similar to those we proposed for the solution of the Navier–Stokes equations, and the full coupling between the different physical phenomena is achieved as in the schemes for fluid-structure interaction analysis [20–22].

In the next sections, we first review the general Maxwell's equations and the form in which we use these equations for our discretization scheme. We pursue static and harmonic solutions, and give some attention to the boundary conditions that arise in practice. Since we consider the solution using primitive variables and potentials, and two- and three-dimensional analyses, the use of the appropriate formulation can be important. Finally, we present the results of some fluid and structural problems with electromagnetic effects that illustrate the procedures proposed in this paper.

2. The electromagnetic governing equations

In this section we first summarize the original first-order Maxwell's equations, and then focus on the reformulation of the equations to the form in which we are solving them using a novel finite element scheme for electromagnetics (but previously published for fluid flows [19]). In a typical analysis, we consider the electric, magnetic, fluid and structural domains, possibly with heat transfer.

The computational domain can be two- or three-dimensional, and in total may consist of an electric domain Ω_e and/or magnetic domain Ω_m. In general, the coupled analysis also includes the structural domain, Ω_s, and the fluid domain, Ω_f. These domains may be partially or fully coincident, as illustrated in Fig. 1.

In the following we focus on the electromagnetic effects, but also discuss how these effects are coupled into the structural and fluid flow phenomena. For the solution of the fluid flows and structural responses, the discretizations used and the coupling procedures, we refer to refs. [19–23].

2.1. Original Maxwell's equations

The original first-order full Maxwell's equations [24], in general static or time-varying fields, can be written as Faraday's law

$$\nabla \times \mathbf{E} = -\mathbf{K} \tag{1}$$

and Ampère's law with the Maxwell term

$$\nabla \times \mathbf{H} = \mathbf{J} \tag{2}$$

where **E** and **H** are the electric and magnetic field intensities, and **J** and **K** are electric and magnetic current density source terms given below.

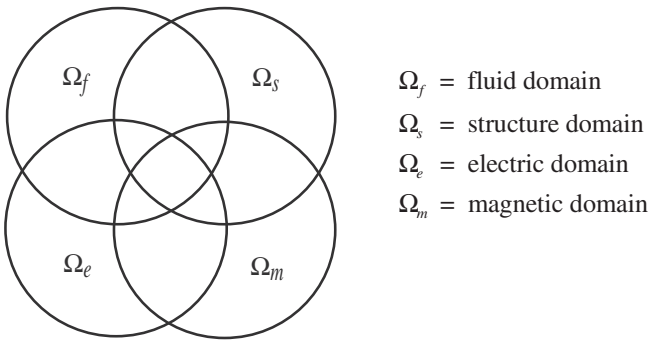

Fig. 1. Schematic diagram of physical domains that can be considered; the domain disks can be moved and any one of the domains may not be present.

The additional equations are the Gauss law applied to the electric and magnetic fields

$$\nabla \cdot \mathbf{D} = \rho_0 \tag{3}$$

$$\nabla \cdot \mathbf{B} = 0 \tag{4}$$

where

$$\mathbf{D} = \varepsilon \mathbf{E}, \quad \mathbf{B} = \mu \mathbf{H} \tag{5}$$

and ε, μ are the permittivity and permeability, respectively, of the material in the fields, and ρ_0 is a charge density source (the value being dependent on the equation).

Here we have

$$\begin{aligned} \mathbf{J} &= \mathbf{J}_0 + \sigma \mathbf{E} + \frac{\partial \mathbf{D}}{\partial t} \\ \mathbf{K} &= \mathbf{K}_0 + \frac{\partial \mathbf{B}}{\partial t} \end{aligned} \tag{6}$$

where $\mathbf{J}_0$ and $\mathbf{K}_0$ are the imposed electric and magnetic current densities respectively, and σ is the electric conductivity of the medium.

In the above equations, we do not point out the domains in which the variables are computed, because the context itself will imply where the variables are applicable. For the same reason, we also do not specify the individual computational domains in the following.

We consider the harmonic and static cases. In a harmonic analysis, all variables are expressed as $\mathrm{Re}(f^* e^{i\omega t})$ with a prescribed angular frequency ω, $f^* = f_r + i f_i$ where i is the imaginary unit, and we have in phasor form

$$\begin{aligned} \mathbf{J} &= \mathbf{J}_0 + i\omega \varepsilon^* \mathbf{E} \\ \mathbf{K} &= \mathbf{K}_0 + i\omega \mathbf{B} \end{aligned}$$

where $\varepsilon^* = \varepsilon - i\sigma/\omega$.

In static analysis, naturally, all time-dependent terms vanish and all imaginary components are not present.

We should also note that, once the complex response has been calculated, the actual solution is given by

$$f = f_r \cos \omega t - f_i \sin \omega t$$

In our numerical solutions we solve for f_r and f_i using real arithmetic.

2.2. *E–H* formulation of Maxwell's equations for finite element solution

The second-order equation system is obtained by applying the operator $\nabla\times$ to Eqs. (1) and (2) to obtain

$$\nabla \times \nabla \times \mathbf{E} = -\nabla \times \mathbf{K} \tag{7}$$

$$\nabla \times \nabla \times \mathbf{H} = \nabla \times \mathbf{J} \tag{8}$$

Introducing as additional solution variables

$$p = \nabla \cdot \mathbf{E} - \rho_0/\varepsilon^* \tag{9}$$

$$q = \nabla \cdot \mathbf{H} \tag{10}$$

Eqs. (7) and (8) can be written as

$$\nabla \cdot ((p + \rho_0/\varepsilon^*)\mathbf{I} - \nabla \mathbf{E} + \mathbf{I} \times \mathbf{K}) = \mathbf{0} \tag{11}$$

and

$$\nabla \cdot (q\mathbf{I} - \nabla \mathbf{H} - \mathbf{I} \times \mathbf{J}) = \mathbf{0} \tag{12}$$

where **I** is the identity tensor.

Eqs. (11), (12), (3), and (4) form the **E**–**H** mathematical formulation that we use for our finite element solution. This formulation is specialized to specific cases, when appropriate, by omitting certain equations. We note that we use the divergence form of the

governing equations to directly satisfy conservation in our formulation like in the FCBI formulation of fluid flows [19–22], and indeed to solve these equations we employ the same weight and interpolation functions and control volumes as in the fluid flow formulations (but, of course, without introducing upwinding because there are no convection terms).

Of course, this second-order equation system is equivalent to the first-order system, if proper boundary conditions are used (see Section 3). With the **E**–**H** formulation, we calculate the Lorentz force and Joule heating rate directly (to couple into the structural and fluid flow response) without further differentiation. However, the formulation may not be convenient if we only know potentials as boundary conditions, in which case the use of a potential formulation is more direct.

2.3. **A**–ϕ potential formulation of Maxwell's equations for finite element solution

As is standard, we introduce the electric and magnetic potentials ϕ and **A** [24]

$$\begin{aligned}\mathbf{E} &= -\nabla\phi - \frac{\partial \mathbf{A}}{\partial t}\\ \mathbf{B} &= \nabla \times \mathbf{A}\end{aligned} \tag{13}$$

and assume

$$\nabla \cdot \mathbf{A} = g_A \tag{14}$$

where

$$g_A = \begin{cases} 0 & \text{Coulomb gauge approximation}\\ -i\mu\varepsilon\omega\phi & \text{Lorenz gauge approximation}\end{cases}$$

Eqs. (1) and (4) are then automatically satisfied (assuming $\mathbf{K}_0 = \mathbf{0}$), and Eqs. (2) and (3) become, respectively, in harmonic analysis

$$\nabla \cdot (-\varepsilon^*(\nabla\phi + i\omega\mathbf{A})) = \rho_0 \tag{15}$$

$$\nabla \times (\mu^{-1}\nabla \times \mathbf{A}) = \mathbf{J}_0 - i\omega\varepsilon^*(\nabla\phi + i\omega\mathbf{A}) \tag{16}$$

Eq. (16) can be written in conservation form

$$\nabla \cdot ((r + \mu^{-1}g_A)\mathbf{I} - \mu^{-1}\nabla\mathbf{A}) = \mathbf{J}_0 - i\omega\varepsilon^*(\nabla\phi + i\omega\mathbf{A}) \tag{17}$$

where

$$r = \mu^{-1}(\nabla \cdot \mathbf{A} - g_A) \tag{18}$$

As for the **E**–**H** mathematical formulation, these equations are specialized to specific cases, as appropriate, by omitting certain equations, and are solved using the approach of the fluid flow solution scheme [19]. The potential-based **A**–ϕ formulation is more appropriate than the **E**–**H** formulation when we know potentials as boundary conditions. However, the physically interesting field quantities **E** and **H** are then computed by differentiation, which introduces numerical errors. A specific advantage of the potential-based formulation is that we solve in three-dimensional analyses only for 5 ($\mathbf{A}, \phi, r$) and 10 unknown components in static and harmonic analyses, respectively, compared with 8 ($\mathbf{E}, \mathbf{H}, p, q$) and 16 unknown components in the **E**–**H** formulation.

2.4. Scales for non-dimensionalization

Before a discretization is performed, it can be important to recast the governing equations (of course, including the boundary and interface conditions) to the use of non-dimensional variables. We have found it effective to use the following variable scales: the length (L_*), permeability (μ_*), permittivity (ε_*) and magnetic field intensity (H_*) with

$$\begin{aligned}E_* &= H_*\sqrt{\mu_*/\varepsilon_*}\\ \sigma_* &= L_*^{-1}\sqrt{\varepsilon_*/\mu_*}\\ \rho_{0^*} &= E_*\varepsilon_*/L_*\\ J_{0^*} &= H_*/L_*\\ K_{0^*} &= E_*/L_*\\ \omega_* &= 1/(L_*\sqrt{\mu_*\varepsilon_*})\\ A_* &= \mu_* H_* L_*\\ \phi_* &= E_* L_*\end{aligned} \tag{19}$$

It is sometimes more efficient to choose the conductivity σ instead of ε as an independent scale. In this case, we use the permittivity scale as $\varepsilon_* = \mu_*(L_*\hat{\sigma})^2$ where $\hat{\sigma}$ is a typical value of conductivity in the model.

3. Boundary and interface conditions

A particularly important aspect of electromagnetic analysis is the imposition of the proper boundary and interface conditions. These conditions should be satisfied for both field intensities, **E** and **H**, and, if used, potentials **A** and ϕ.

3.1. Boundary conditions

Considering first the essential boundary conditions of prescribing values (the Dirichlet boundary conditions) we have

$$\mathbf{v} = \mathbf{v}_b \quad (\mathbf{v} = \mathbf{E}, \mathbf{H}, \mathbf{A}, \phi) \tag{20}$$

on all components of the variable **v**.

This type of boundary condition may be applied only to the normal component of a vector variable (called also 'normal condition')

$$\mathbf{n} \cdot \mathbf{v} = v_b \quad (\mathbf{v} = \mathbf{E}, \mathbf{H}, \mathbf{A}) \tag{21}$$

or only to the tangential components of a vector variable (called also 'parallel condition')

$$\mathbf{n} \times \mathbf{v} = v_b\mathbf{d} \quad (\mathbf{v} = \mathbf{E}, \mathbf{H}, \mathbf{A}) \tag{22}$$

where **n** is the outward unit normal to the boundary and **d** is the specified direction.

Electric and magnetic boundary conditions are frequently combined in practical applications. For example, in the *odd symmetry* condition, we impose $\mathbf{n} \cdot \mathbf{H} = 0$ and $\mathbf{n} \times \mathbf{E} = \mathbf{0}$, and in the *even symmetry* condition we impose $\mathbf{n} \cdot \mathbf{E} = 0$ and $\mathbf{n} \times \mathbf{H} = \mathbf{0}$.

Further, we also have the two equivalent impedance conditions in harmonic analysis,

$$\mathbf{n} \times \mathbf{E} = -Z_s\mathbf{n} \times (\mathbf{n} \times \mathbf{H}) \tag{23}$$

and

$$\mathbf{n} \times \mathbf{H} = Z_s^{-1}\mathbf{n} \times (\mathbf{n} \times \mathbf{E}) \tag{24}$$

applicable to **E** and **H** respectively, in which Z_s is the surface impedance (a complex number).

The impedance condition for the magnetic potential **A** is

$$\mathbf{n} \times (\nabla \times \mathbf{A}) = -\mu Z_s^{-1}\mathbf{n} \times (\mathbf{n} \times (\nabla\phi + i\omega\mathbf{A})) \tag{25}$$

This type of boundary condition covers some other practical cases. One of them is the finite conductivity condition that is used to model good conductors. In this case, $\delta = \left(\frac{1}{2}\omega\mu\sigma\right)^{-\frac{1}{2}}$ and the impedance is given by

$$Z_s = (1+i)(\delta\sigma)^{-1} = (1+i)(\omega\mu/(2\sigma))^{\frac{1}{2}} \tag{26}$$

Another one is the lumped *RLC*-boundary condition used to model, for example, a lumped resistor or inductor.

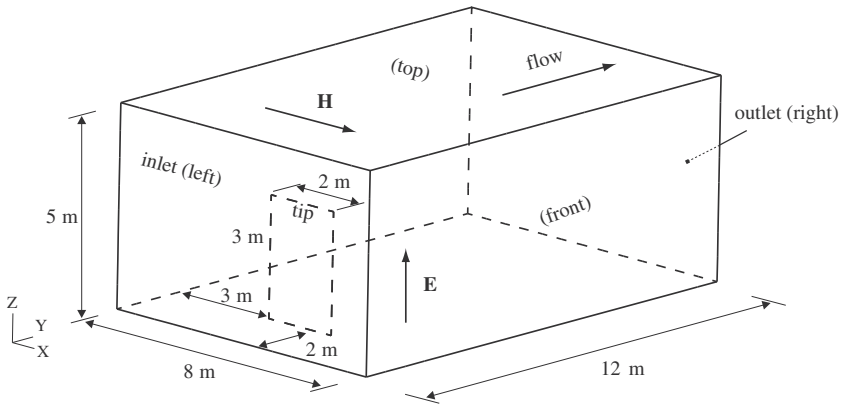

Fig. 2. Schematic of shell structure, thickness = 1.25 mm, in fluid flow in an electromagnetic pump.

Table 1
Material properties in driven electromagnetic pump.

EM properties	
Permittivity (ε)[F/m]	ε_0
Permeability (μ)[H/m]	μ_0
Electric conductivity (σ)[S/m]	100
Fluid properties	
Density [kg/m^3]	1000
Viscosity [kg/m–s]	0.1
Solid properties	
Young's modulus [Gpa]	70
Poisson's ratio	0.3

The impedance condition can also be used for simulating certain absorbing boundary conditions, as illustrated in the example in Section 6.4.

In addition, since we solve the second-order Maxwell's equations, we also have to impose the first-order Eqs. (1) to (4) when necessary, as natural boundary conditions.

Finally, the variables p and q are imposed to be zero on all boundaries.

3.2. Interface conditions

On a material interface, the following interface conditions need special attention in the computational procedure

$$\begin{aligned}
&\mathbf{n}\times\mathbf{E}_L = \mathbf{n}\times\mathbf{E}_R\\
&\mathbf{n}\times\mathbf{H}_L = \mathbf{n}\times\mathbf{H}_R\\
&\mathbf{n}\cdot(\varepsilon^*\mathbf{E})_L = \mathbf{n}\cdot(\varepsilon^*\mathbf{E})_R\\
&\mathbf{n}\cdot(\mu\mathbf{H})_L = \mathbf{n}\cdot(\mu\mathbf{H})_R
\end{aligned} \tag{27}$$

where $(\cdot)_L$ and $(\cdot)_R$ represent the variables on the two sides of the interface respectively.

4. Finite element discretization of governing equations

Considering Eqs. (11) and (12), and the boundary conditions, a close resemblance to the Navier–Stokes equations of incompressible fluid flows without the convective terms is noticed [23]. Hence, we solve these equations using the finite element interpolations that we use for fluid flow solutions, see refs. [19–23]. Of course, the p and q variables are special but the interpolation approach is directly applicable, and used similarly as for the pressure in fluid flows [23].

5. Coupling to structures and fluids

The coupling occurs for domains in which the structural, fluid and electromagnetic variables are active. In these domains, the Maxwell stresses and Joule heating rate are calculated and added to the stresses and the energy sources, respectively, for the structural and fluid flow solutions, meaning that, in general, heat transfer conditions are also solved for in the structural and fluid flow domains [4]. The coupling is achieved like in coupled fluid-flow, heat transfer, structural interaction solutions [20–22].

The coupled fluid and structural solutions can be obtained in steady-state and transient analyses, irrespective of the analysis type for the electromagnetic model. In a static electromagnetic analysis, the electromagnetic force and heat source are constant for the fluid flow and structural models. On the other hand, if the electromagnetic solution corresponds to a harmonic analysis, then

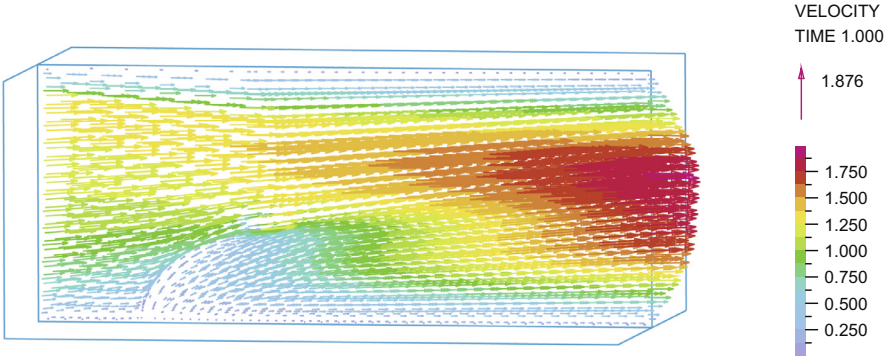

Fig. 3. Velocity field in an intersection plane of the flow domain of the electromagnetic pump.

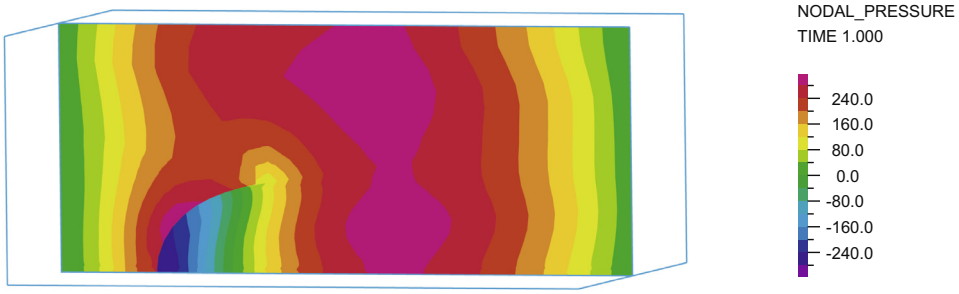

Fig. 4. Pressure distribution in an intersection plane of the flow domain of the electromagnetic pump.

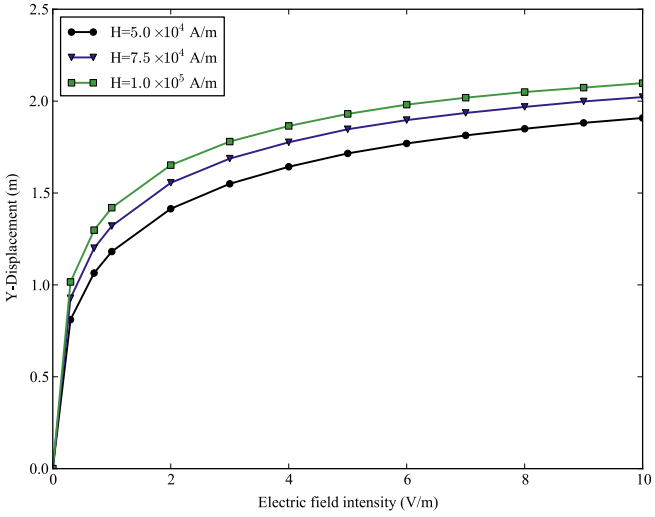

Fig. 5. Structure tip displacement as function of electric and magnetic field intensities.

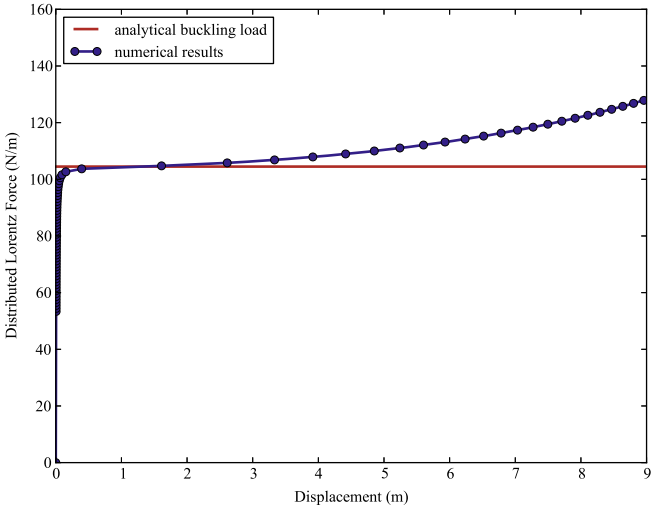

Fig. 7. Buckling and large displacement response of the beam due to Lorentz force.

averaged electromagnetic forces and Joule heating (over one period, see below) are usually used.

5.1. Lorentz force and Maxwell stresses

The Lorentz body force $\mathbf{f}_b^{em}$ per unit volume, used in our formulation as a body force, can be expressed in terms of the Maxwell stresses

$$\mathbf{f}_b^{em} = \nabla \cdot \mathbf{T}^{em} + \mathbf{T}_b^{em} \tag{28}$$

where the Maxwell stresses $\mathbf{T}^{em}$ and $\mathbf{T}_b^{em}$ are

$$\begin{aligned} \mathbf{T}^{em} &= \mathbf{T}^{e} + \mathbf{T}^{m} \\ \mathbf{T}^{e} &= \mathbf{DE} - \frac{1}{2}(\mathbf{D}\cdot\mathbf{E})\mathbf{I} \\ \mathbf{T}^{m} &= \mathbf{BH} - \frac{1}{2}(\mathbf{B}\cdot\mathbf{H})\mathbf{I} \\ \mathbf{T}_b^{em} &= -\frac{\partial \mathbf{D}\times\mathbf{B}}{\partial t} \end{aligned} \tag{29}$$

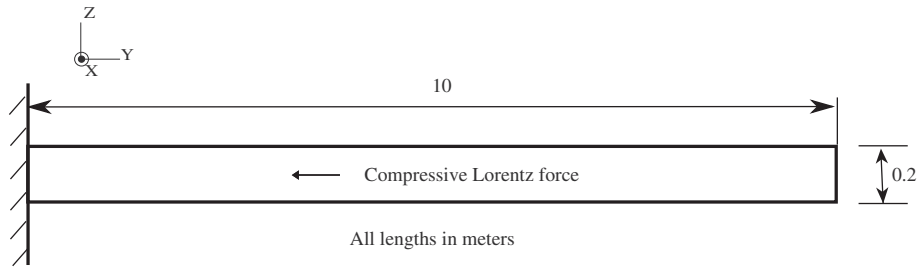

Structure: Elastic material

$E = 1.0 \times 10^8\ N/m^2$

$\nu = 0.0$

Electromagnetic material:

$\mu = 1.25 \times 10^{-6}\ H/m$

$\sigma = 1.0 \times 10^6\ S/m$

Fig. 6. Beam subjected to compressive Lorentz force.

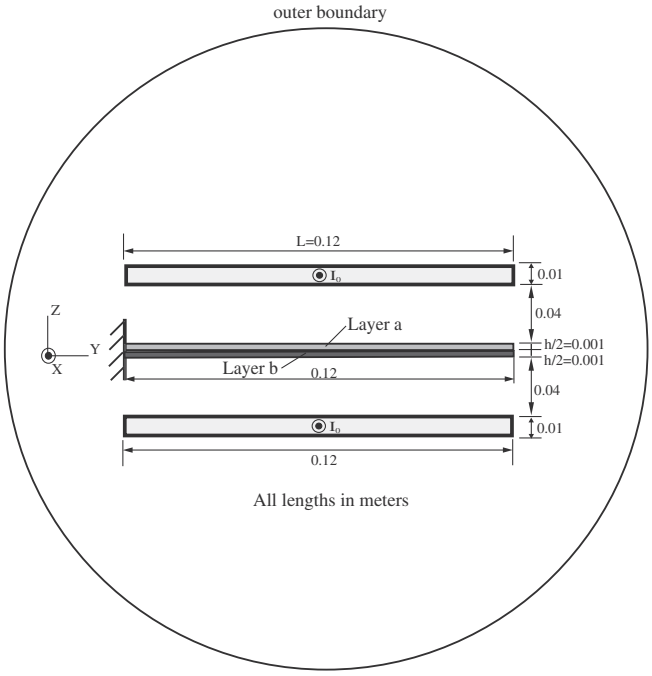

Fig. 8. Schematic figure of the bimetallic beam and the plates carrying the imposed AC current; the diameter of the modeled domain is 1.2 m.

In the **E–H** formulation, the calculated variables are directly used in Eq. (29), while in the **A**–ϕ formulation, the field intensities are calculated using Eq. (13) and then used in Eq. (29).

Of course, if only the electric field is active, then $\mathbf{T}^m$ and $\mathbf{T}_b^{em}$ are omitted, and similarly, if only the magnetic field is active, $\mathbf{T}^e$ and $\mathbf{T}_b^{em}$ are omitted.

5.2. Joule heating rate

The heat source generated by electromagnetic variables is calculated as

$$q_b^{em} = \sigma^{-1}\mathbf{J}\cdot\mathbf{J} \tag{30}$$

in which **J** is given by Eq. (6).

Table 2
Material properties of the bimetallic beam.

Properties	Layer a	Layer b	Plates	Outer space
Density [kg/m^3]	8000	7800	-	-
Young's modulus [Gpa]	141	210	-	-
Poisson's ratio	0	0	-	-
Thermal expansion coefficient [1/K]	10^{-6}	4×10^{-5}	-	-
Thermal conductivity [W/m–K]	10	30	-	-
Specific heat [J/kg–K]	500	1000	-	-
Electric conductivity (σ)[S/m]	6×10^7	6×10^7	10^7	0
Permeability (μ)[H/m]	μ_0	μ_0	μ_0	μ_0
Permittivity (ε)[F/m]	ε_0	ε_0	ε_0	ε_0

5.3. Coupling effects in harmonic analysis

In harmonic analyses, the Maxwell stress and Joule heating rate are time-varying, so they can be directly computed at any specified time. According to the definitions in Eqs. (29) and (30)

$$\begin{aligned}
\mathbf{T}^e &= \mathrm{Re}(\mathbf{D}e^{i\omega t})\mathrm{Re}(\mathbf{E}e^{i\omega t}) - \frac{1}{2}\mathrm{Re}(\mathbf{D}e^{i\omega t})\cdot\mathrm{Re}(\mathbf{E}e^{i\omega t})\mathbf{I}\\
\mathbf{T}^m &= \mathrm{Re}(\mathbf{B}e^{i\omega t})\mathrm{Re}(\mathbf{H}e^{i\omega t}) - \frac{1}{2}\mathrm{Re}(\mathbf{B}e^{i\omega t})\cdot\mathrm{Re}(\mathbf{H}e^{i\omega t})\mathbf{I}\\
\mathbf{T}_b^{em} &= \omega[\mathrm{Re}(\mathbf{D}e^{i\omega t})\times\mathrm{Im}(\mathbf{B}e^{i\omega t}) + \mathrm{Im}(\mathbf{D}e^{i\omega t})\times\mathrm{Re}(\mathbf{B}e^{i\omega t})]
\end{aligned} \tag{31}$$

and

$$q_b^{em} = \sigma^{-1}\mathrm{Re}(\mathbf{J}e^{i\omega t})\cdot\mathrm{Re}(\mathbf{J}e^{i\omega t}) \tag{32}$$

However, the time-averaged values (over one period) are actually frequently used in solutions

$$\bar{f} = \frac{1}{2\pi}\int_0^{2\pi} f\, d(\omega t) \tag{33}$$

Then Eqs. (29) and (30) become, respectively,

$$\begin{aligned}
\bar{\mathbf{T}}^{em} &= \bar{\mathbf{T}}^e + \bar{\mathbf{T}}^m\\
\bar{\mathbf{T}}^e &= \frac{1}{2}(\mathbf{D}_r\mathbf{E}_r + \mathbf{D}_i\mathbf{E}_i) - \frac{1}{4}(\mathbf{D}_r\cdot\mathbf{E}_r + \mathbf{D}_i\cdot\mathbf{E}_i)\mathbf{I}\\
\bar{\mathbf{T}}^m &= \frac{1}{2}(\mathbf{B}_r\mathbf{H}_r + \mathbf{B}_i\mathbf{H}_i) - \frac{1}{4}(\mathbf{B}_r\cdot\mathbf{H}_r + \mathbf{B}_i\cdot\mathbf{H}_i)\mathbf{I}\\
\bar{\mathbf{T}}_b^{em} &= \mathbf{0}
\end{aligned} \tag{34}$$

and

$$\bar{q}_b^{em} = \frac{1}{2}\sigma^{-1}(\mathbf{J}_r\cdot\mathbf{J}_r + \mathbf{J}_i\cdot\mathbf{J}_i) \tag{35}$$

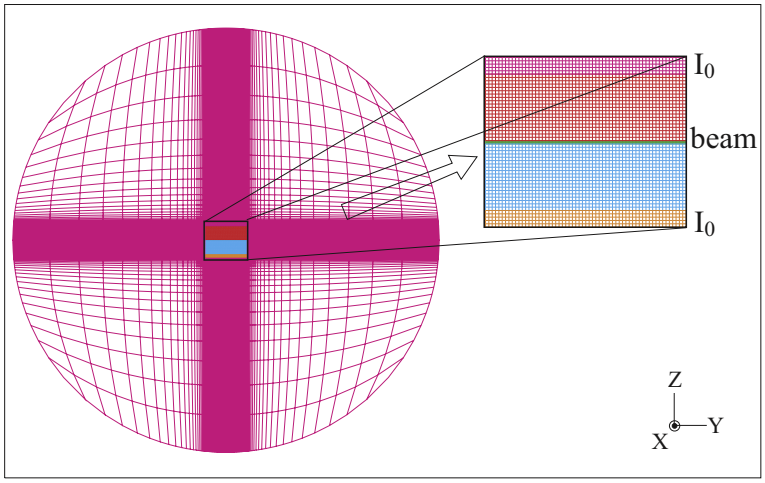

Fig. 9. Mesh for electromagnetic analysis spanning over the beam, plates, and far domain.

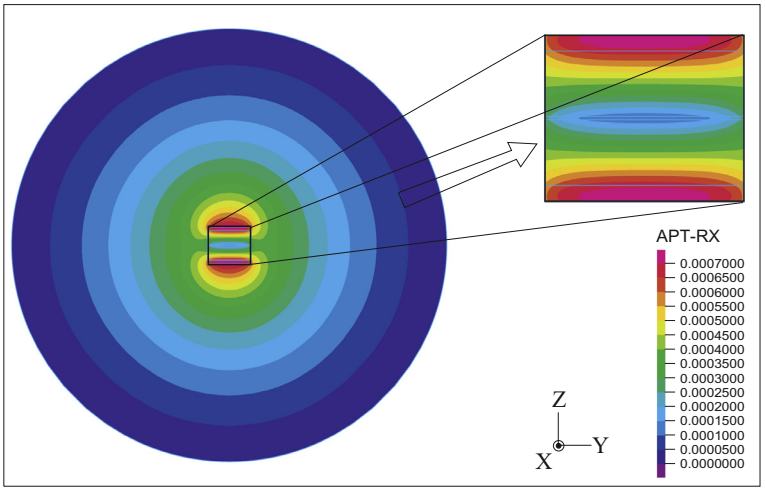

Fig. 10. Real component of magnetic potential at $I_0 = 2 \times 10^3$ A and $f = 60$ Hz.

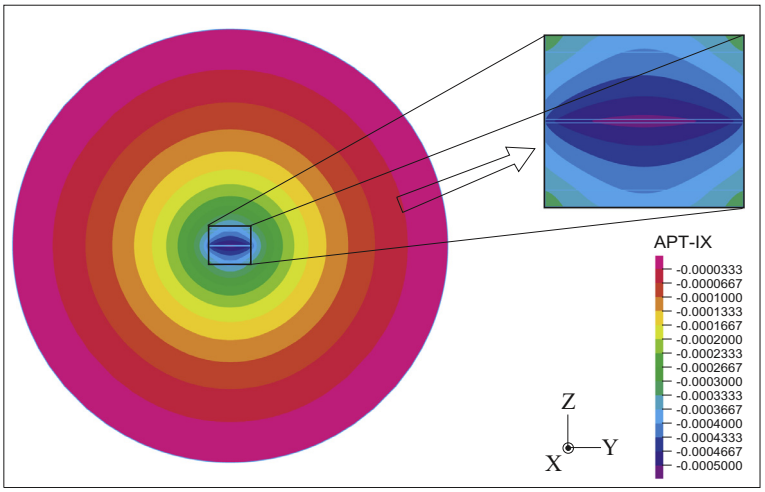

Fig. 11. Imaginary component of magnetic potential at $I_0 = 2 \times 10^3$ A and $f = 60$ Hz.

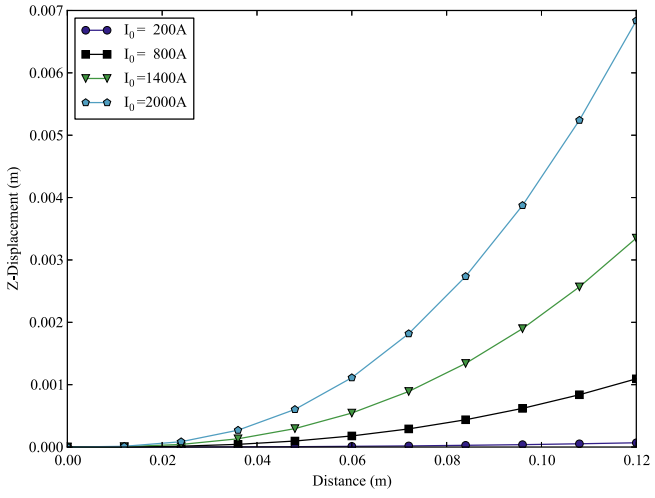

Fig. 12. Beam transverse displacement for different imposed currents and $f = 60$ Hz.

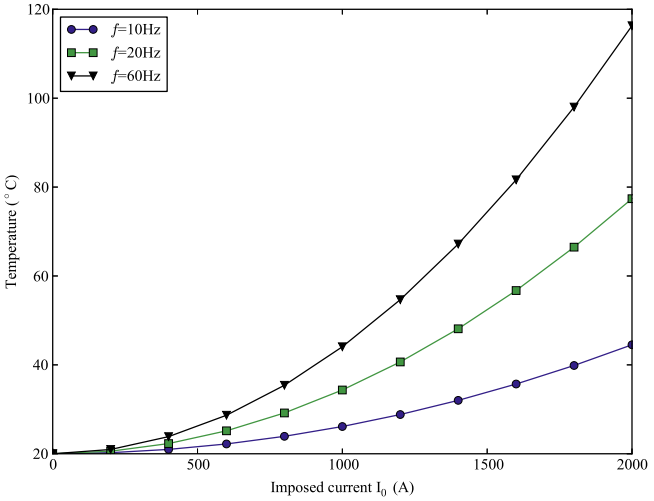

Fig. 13. Temperature in beam as a function of imposed current, for different frequencies.

6. Illustrative example solutions

In this section we present various problem solutions to illustrate the applicability of the solution schemes. In the example solutions we use the free space permeability $\mu_0 = 1.25 \times 10^{-6}$H/m and permittivity $\varepsilon_0 = 8.854 \times 10^{-12}$F/m, and the frequency $f = \omega/(2\pi)$. If not explicitly mentioned, ρ_0, $\mathbf{J}_0$, and $\mathbf{K}_0$ are zero.

6.1. Thin structure in a Lorentz force driven electromagnetic pump

We consider a cantilevered thin shell structure in a channel of an electromagnetic pump, see Fig. 2. The fluid flow in the pump is driven by the Lorentz force from the electromagnetic fields. A similar problem was solved in refs. [21,25], where no electromagnetic effects were included. In this problem, the Lorentz body force, Maxwell stress balance the fluid stress and drive the fluid flow. Fig. 2 shows the directions of the magnetic and electric field intensities across the domain and the driven flow direction in the electromagnetic pump. The electromagnetic, fluid and solid material properties are listed in Table 1.

The electromagnetic computational domain corresponds to the union of the fluid and solid domains. The boundary conditions are that the electric field intensity **E** is prescribed on the bottom surface in the vertical direction from 0 to 10 V/m, $\mathbf{n} \times \mathbf{E} = \mathbf{0}$ on the top surface, and $\mathbf{n} \cdot \mathbf{E} = 0$ on the rest of the bounding surfaces; **H** is prescribed in the *X*-direction at the fluid inlet (left) surface from 50,000 A/m to 100,000 A/m, $\mathbf{n} \times \mathbf{H} = \mathbf{0}$ on the front and back surfaces, and $\mathbf{n} \cdot \mathbf{H} = 0$ on the rest of the external surfaces. For the fluid variables, zero ambient pressure is prescribed at the inlet (left) and outlet (right) surfaces, and the no-slip wall condition is imposed at the channel walls.

The electromagnetic variables **E**–**H** are solved for using 8-node elements; the shell structure is modeled using 27-node solid elements; and the fluid flow is modeled using 8-node FCBI-C elements [21,22]. In this problem, the magnetic Reynolds number is small and hence the fluid flow has little effect on the electric and magnetic fields. On the other hand, since the flow Reynolds number is high, we use the k–ε turbulence model for the fluid flow.

Figs. 3 and 4 show typical velocity field and pressure distributions in a cross section for the *X*-direction view. As expected, the wake fluid field behind the shell structure and the pressure discontinuity across the shell structure are present. Fig. 5 shows the structure tip displacement as a function of the applied electric and magnetic field intensities. The figure clearly shows that, as also expected, the shell structural displacements become nonlinearly larger as the electric and magnetic field intensities increase.

6.2. Beam buckling due to Lorentz force

Here we consider the buckling and large displacement response of a beam subjected to an applied Lorentz body force, see Fig. 6 for the geometric dimensions and material properties. A constant magnetic field intensity and varying electric field intensity result in an almost linear increase of the Lorentz body force. The static **E**–**H** formulation is used for the electromagnetic computational domain which is coincident with the structural domain.

The beam, as shown in Fig. 6, is fixed at its left end. The structure is modeled using 9-node two-dimensional solid elements. **E** is prescribed in the negative vertical direction on the bottom from 0 to 0.0015 V/m, $\mathbf{n} \times \mathbf{E} = \mathbf{0}$ at the top, and the natural boundary conditions are applied to the left and the right ends of the computational domain; the magnetic field intensity H_X (it is a scalar in this case) is prescribed as 2.09×10^6 A/m at the left end and the natural boundary conditions are applied everywhere else on the boundary.

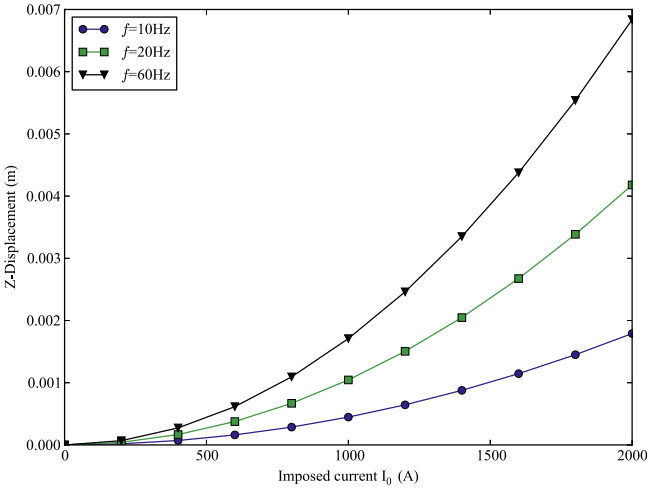

Fig. 14. Tip displacement of beam as a function of imposed current, for different frequencies.

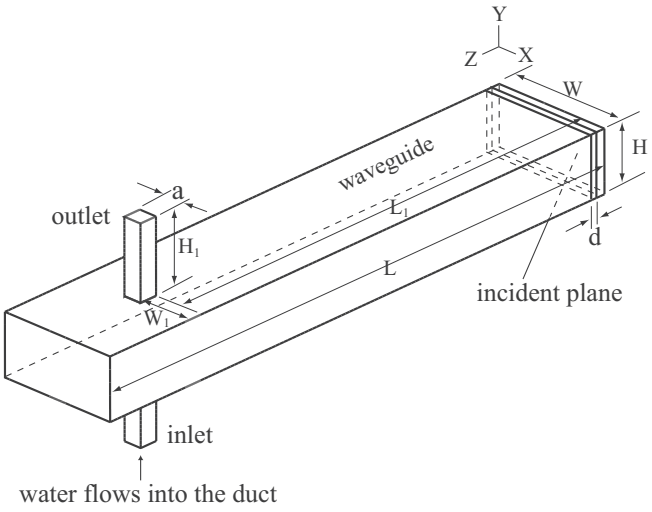

Fig. 15. Schematic figure of the continuous microwave heating system.

Table 3
Dimensions of the waveguide and the flow duct (in meters).

L	W	H	L_1	W_1	H_1	a	d
1.212	0.248	0.124	0.99	0.105	0.15	0.038	0.0001

Table 4
Flow and electromagnetic properties of water.

Properties	Values
Density [kg/m^3]	981.7
Thermal conductivity [W/m–K]	0.7
Specific heat [J/kg–K]	4185.8
Viscosity [kg/m–s]	0.69×10^{-3}
Permittivity (ε)[F/m]	6.336×10^{-10}
Electric conductivity (σ)[S/m]	0.165

An analytical solution of the buckling load due to a spatially constant but increasing body force is given in ref. [26]. Fig. 7 shows the numerically calculated response due to the electromagnetic force and the analytical value of the buckling load. The numerical

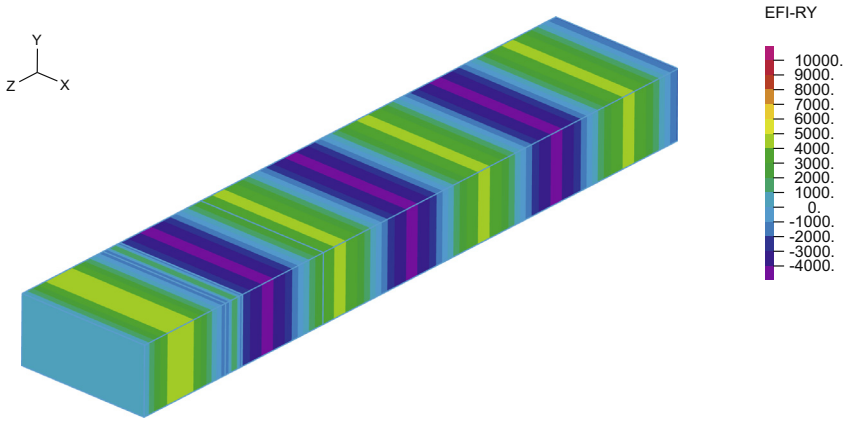

Fig. 16. Calculated real *Y*-component of the electric field intensity.

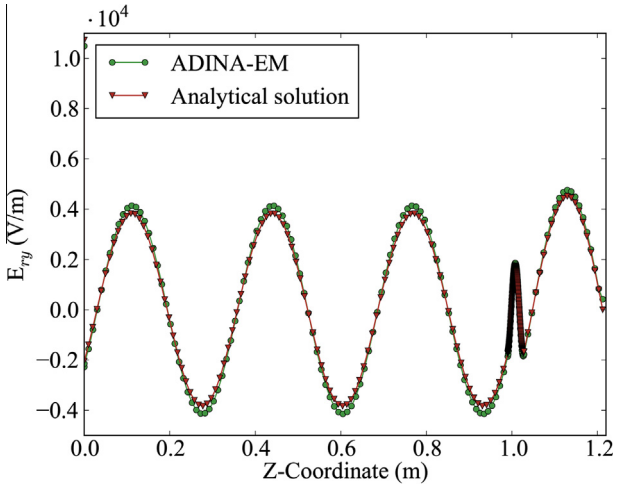

Fig. 17. Calculated real *Y*-component of the electric field intensity and analytical solution.

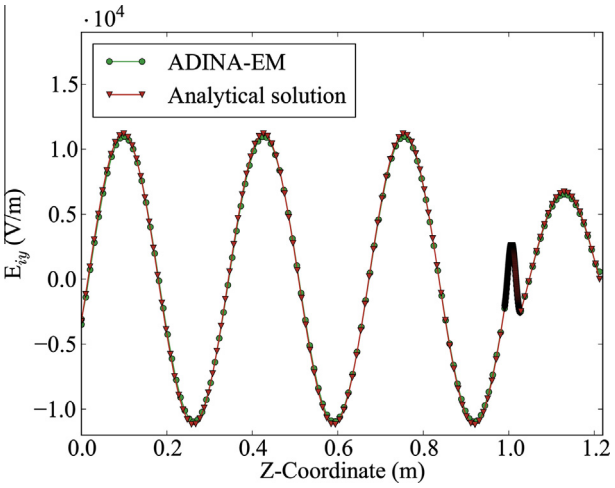

Fig. 19. Calculated imaginary *Y*-component of the electric field intensity and analytical solution.

solution is very close to the analytical buckling load. To reach large displacements an increase in load is needed.

6.3. Bimetallic beam bending due to induction heating

Induction heating is utilized extensively in many industries, for example, for the heat treatment of metals. Here we model a beam in two-dimensional conditions subjected to induction heating, see Fig. 8. The cantilevered beam is made of two layers of different metallic materials and is situated between two plates that carry an AC current. The structure is subjected to induction heating from the eddy currents.

The computational electromagnetic domain includes the two layers of the beam, the two plates onto which the current is imposed, and the outer space. The electromagnetic and solid material properties of the bimetallic beam are listed in Table 2. We use the magnetic potential-based formulation to solve the two-dimensional problem, with the solution variable, a scalar, A_X. The

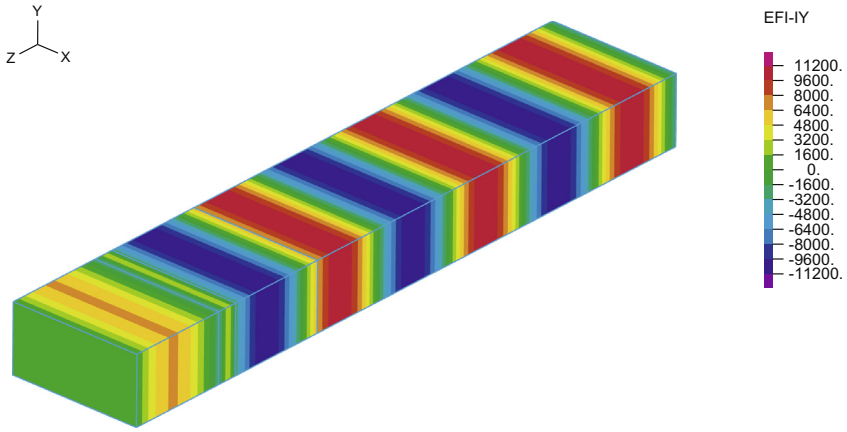

Fig. 18. Calculated imaginary *Y*-component of the electric field intensity.

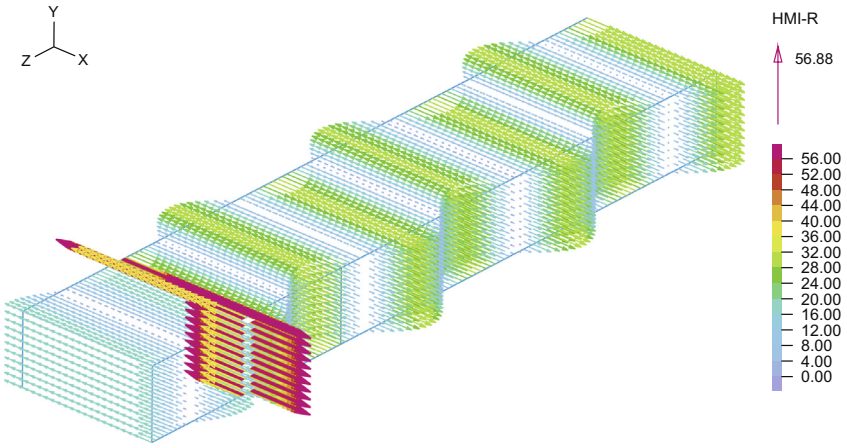

Fig. 20. Calculated real component of the magnetic field intensity vector.

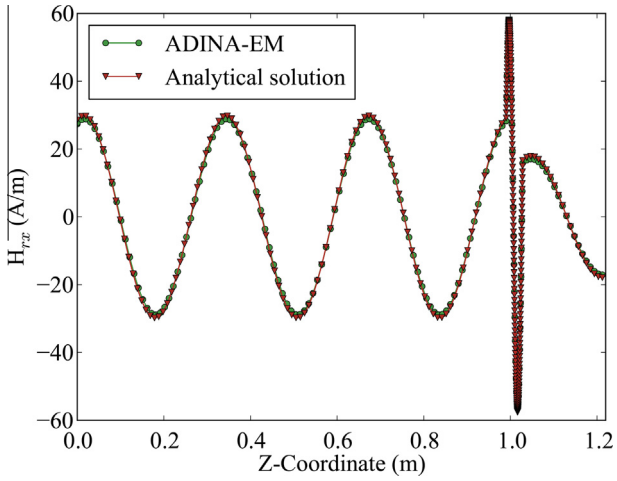

Fig. 21. Calculated real *X*-component of the magnetic field intensity and analytical solution.

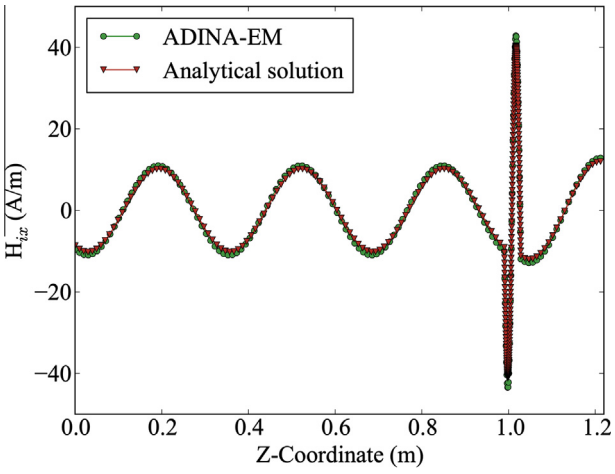

Fig. 23. Calculated imaginary *X*-component of the magnetic field intensity and analytical solution.

imposed current is defined as $\mathbf{I}_0 = \int_S \mathbf{J} \cdot d\mathbf{S}$ where I_0 is the total current in the plate and S is the plate cross-section [27].

Zero potential is prescribed on the outer boundary of the electromagnetic domain. For the heat transfer in the beam, convection boundary conditions are imposed on all free sides of the beam, with the heat convection coefficient 10 W/m^2–K and the environmental temperature 20 ^{0}C. The same temperature is prescribed at the fixed end and set as initial condition as well. A high thermal conductivity is used for the metal materials, and hence the thermal diffusion time is small and the temperature is almost uniform throughout the beam.

Fig. 9 shows the 4-node element mesh used for the electromagnetic solution. The beam is modeled using 9-node solid elements.

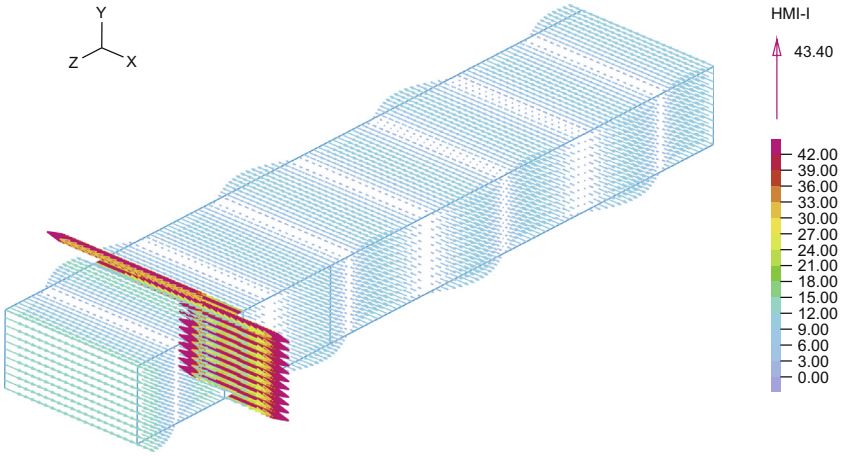

Fig. 22. Calculated imaginary component of the magnetic field intensity vector.

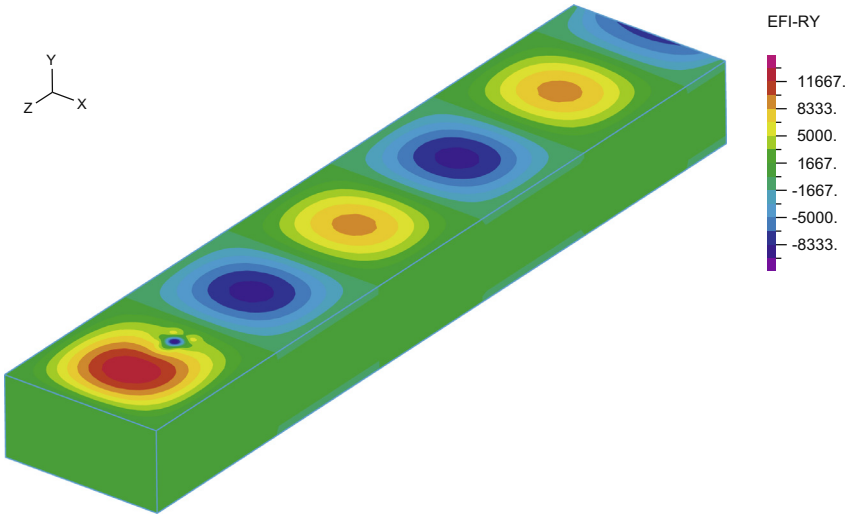

Fig. 24. Calculated real *Y*-component of the electric field intensity.

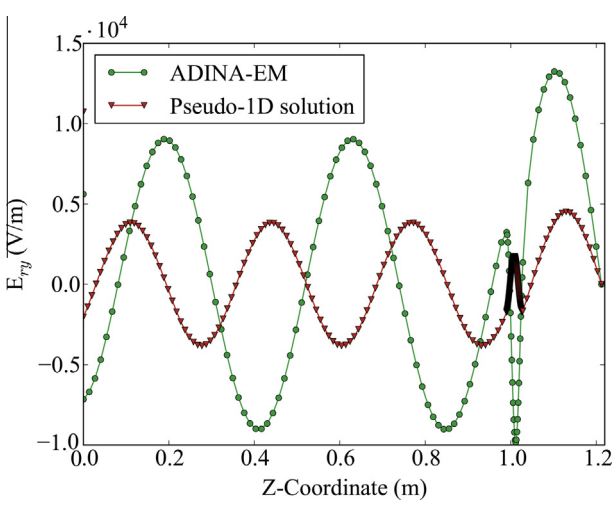

Fig. 25. Comparison of the real *Y*-component of the electric field intensity with pseudo-1D solution.

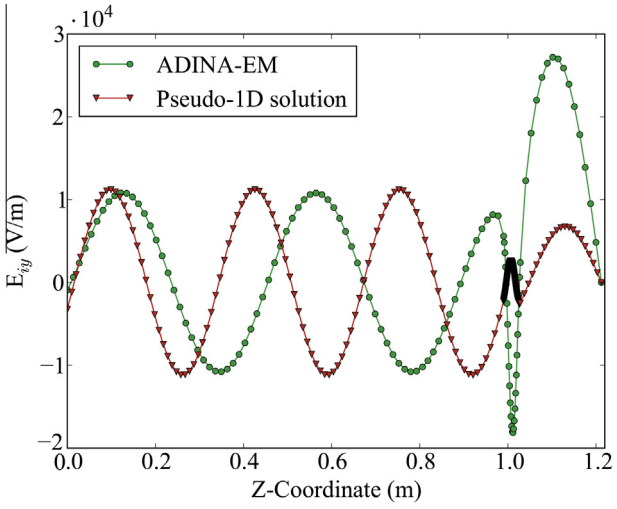

Fig. 27. Comparison of the imaginary *Y*-component of the electric field intensity with pseudo-1D solution.

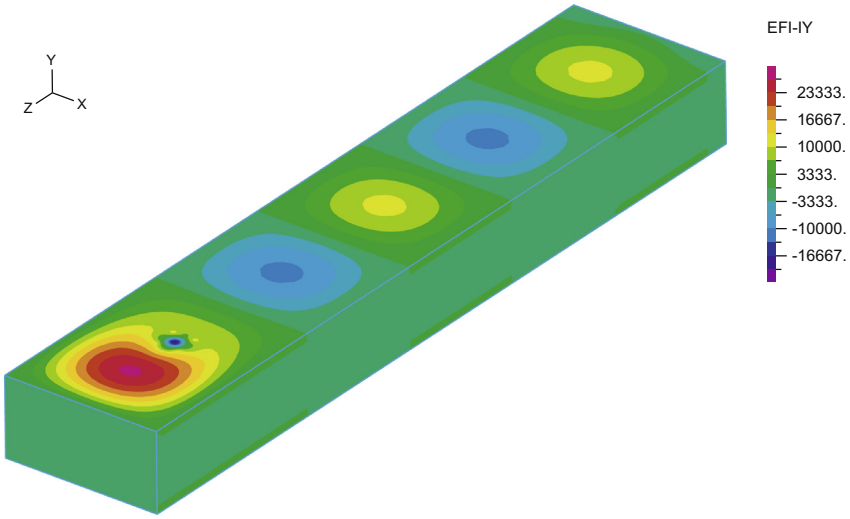

Fig. 26. Calculated imaginary *Y*-component of the electric field intensity.

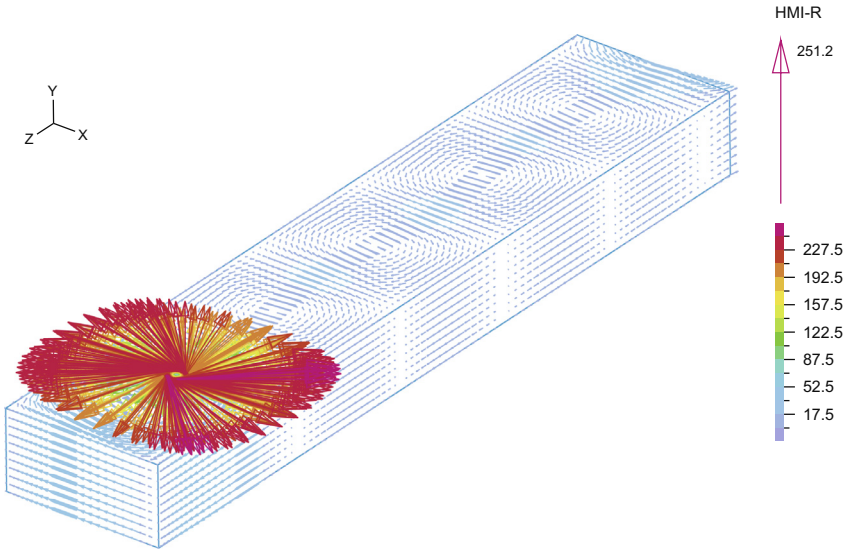

Fig. 28. Calculated real component of the magnetic field intensity vector.

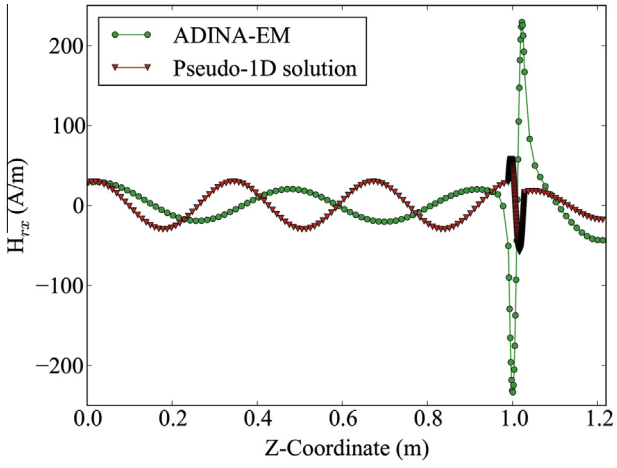

Fig. 29. Comparison of the real *X*-component of the magnetic field intensity with pseudo-1D solution.

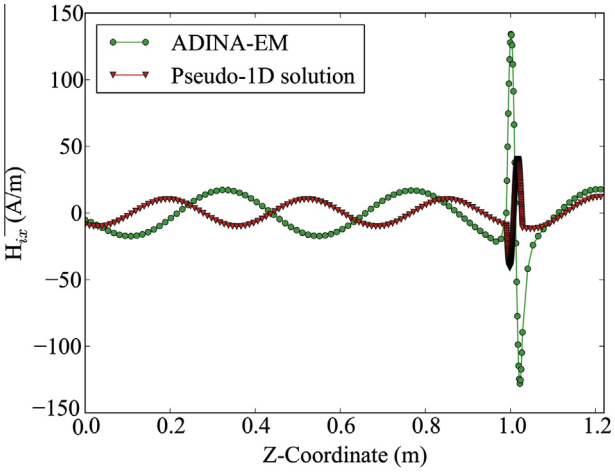

Fig. 31. Comparison of the imaginary *X*-component of the magnetic field intensity with pseudo-1D solution.

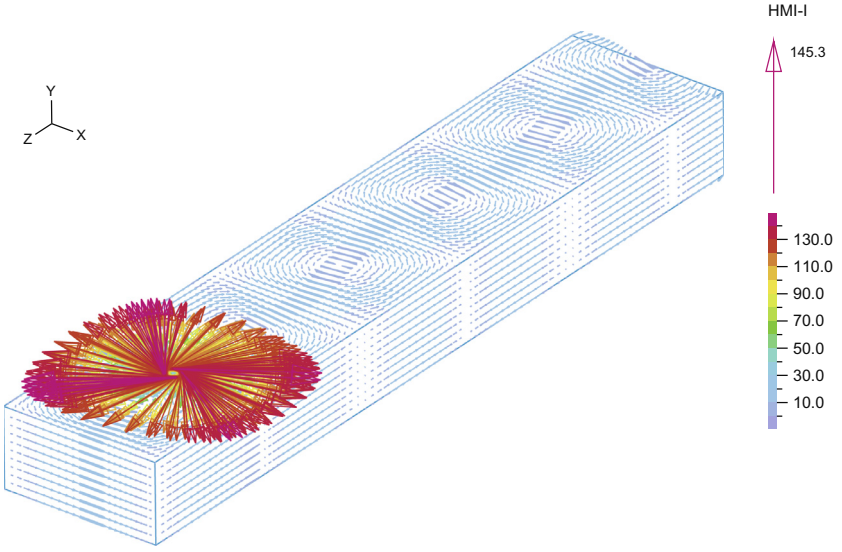

Fig. 30. Calculated imaginary component of the magnetic field intensity vector.

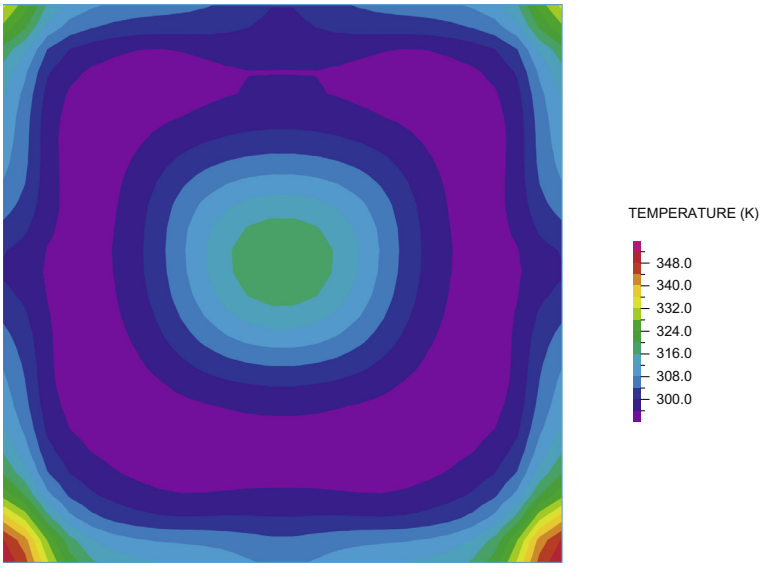

Fig. 32. Temperature distribution in the cross-section of the duct at the mid-plane of the wave guide.

In Figs. 10 and 11 we show the real and imaginary X-components of the magnetic vector potential on the whole domain with insets of the sub-domain containing the beam. In Fig. 12 we give the beam displacement response as a function of the applied electric current at $f = 60$ Hz. Figs. 13 and 14 give the temperature and the tip displacement of the beam, respectively, as a function of the magnitude of the imposed current, at different frequencies.

6.4. Continuous microwave processing of materials

Microwave heating is extensively used for food processing, such as cooking, thawing, tempering and pasteurizing, for ceramics heating, for polymer syntheses, mineral processing, for ablation of human tissues, and other events. In contrast to conventional ways of heating, microwaves heat material samples volumetrically and lead to a faster heat transfer rate and shorter processing time.

We consider the multiphysics analysis of water flowing through a duct in which the water is heated by a guided microwave at the frequency of 915 MHz. Fig. 15 shows the system schematically. The electromagnetic domain is composed of the rectangular waveguide and the duct flow domain. The dimensions of the waveguide and duct are listed in Table 3, the material properties of water are listed in Table 4, and air is assumed to exist in the waveguide. The problem is solved using the **E**–**H** formulation for the electromagnetic response. The water is modeled using the Navier–Stokes equations for incompressible fluid flow.

The waveguide is excited with a 5kW power input through an incident plane wave, which is equivalent to an imposed surface magnetic current density $\mathbf{K}_s = 1.277 \times 10^4 \mathbf{e}_x$V/m [28]. In this analysis, we model the power input by imposing a source $\mathbf{K}_0 = \mathbf{K}_s/d$ in a thin region of thickness d, at the location 0.0001m from the right-end boundary.

At the right end of the waveguide, in order to eliminate the reflection effect, the impedance condition with $Z_s = 377$V/A is applied (to simulate an absorbing boundary condition [29]). On the other enclosing boundaries of the waveguide, perfect electric conduction conditions are assumed.

At the inlet of the fluid flow, the velocity is prescribed, varying between 0.015 m/s and 0.06 m/s, and the temperature is prescribed at 293 K. At the outlet, zero pressure and zero heat flux are specified. The sides of the duct are modeled as no slip adiabatic walls.

In the first part of this study, we solved for the electromagnetic response when the duct is fully extended across the waveguide in the X-direction, that is a = W. For this essentially one-dimensional problem an analytical solution can be obtained. Figs. 16–23 show that the calculated real and imaginary components of the electric and magnetic field intensities using the **E**–**H** formulation are quite close to the analytical solution. This demonstrates that the direct **E**–**H** formulation presented in Section 2.2 can be used for this high-frequency application.

In the second part of the study, the actual flow duct was modeled. Figs. 24–31 show the real and imaginary components of the electric and magnetic field intensities along the centerline of the waveguide. The response is compared with the pseudo-solution mentioned above. It can be seen, from the comparisons, that the flow duct dimensions change the electromagnetic scattering patterns considerably, for both the phases and the magnitudes of the fields. Fig. 32 shows the water temperature at the mid-section plane of the flow duct; we note that the microwave heating is inhomogeneous due to the electromagnetic scattering in the water. Fig. 33 shows how the averaged temperature of the water increases

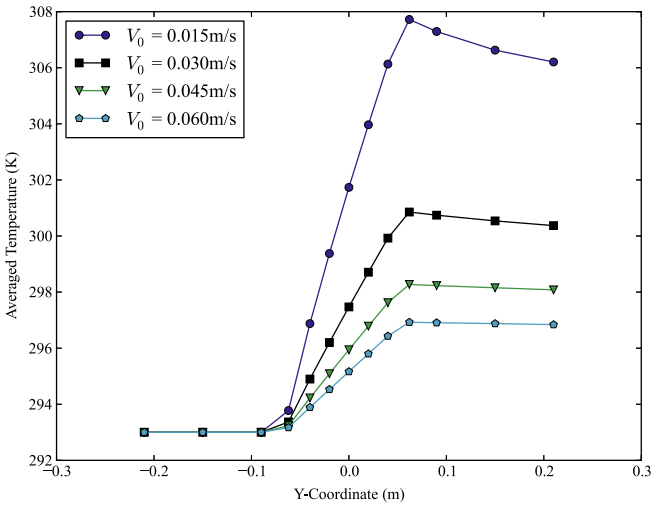

Fig. 33. Averaged water temperature in the duct along flow direction for different inlet velocities V_0.

along the flow duct due to the microwave heating for different inlet velocities.

7. Concluding remarks

The objective in this paper was to present a finite element formulation to include and fully couple electromagnetic effects in the analysis of structures and fluid-structure interactions. The specific attributes of the formulation are that it does not contain spurious solutions, is stable and the finite elements are described by degrees of freedom that can directly be coupled to fluid flow and structural discretizations.

We have illustrated the use of the formulation in the solution of some multiphysics problems. However, the field of electromagnetic analysis is very large and is characterized by numerous different phenomena at varying length and time scales, in particular when these phenomena are coupled to structures and fluid flows. The finite element formulation given here provides a good foundation for studies of some of these phenomena and for further developments to solve with this approach increasingly more complex multiphysics problems.

References

[1] Bathe KJ. The finite element method. In: Wah B, editor. Encyclopedia of computer science and engineering. J. Wiley and Sons; 2009. p. 1253–64.
[2] Li BQ. A finite-element analysis of magnetically driven recirculating flow in electromagnetic near net shape casting. J Mater Process Technol 1995;55:351–9.
[3] Jordan T. Coupling of electromagnetics and structural/fluid dynamics – application to the dual coolant blanket subjected to plasma disruptions. Fusion Technol 1996;30(Part 1):363–71.
[4] Dantzig JA, Roplekar JK, Bhasin AK, Moore JJ, Young YP, Midson S. A mathematical model of the MHD-DC casting process. In: 5th international conference on semi-solid processing of alloys and composites proceedings; 1998. p. 241–48.
[5] Meir AJ, Schmidt PG, El Kaddah N, Robertson DGC, Johansen ST, Voller VR. Analysis and finite element simulation of MHD flows, with an application to liquid metal processing. Fluid Flow Phenom Met Process 1999:561–9.
[6] Sampath R, Zabaras N. Numerical study of convection in the directional solidification of a binary alloy driven by the combined action of buoyancy, surface tension, and electromagnetic forces. J Comput Phys 2001;168:384–411.
[7] Guenneau S, Movchan AB, Poulton CG, Nicolet A. Coupling between electromagnetic and mechanical vibrations of thin–walled structures. Q J Mech Appl Mech 2004;57:407–28.
[8] Chu SC, Lian SS. Numerical analysis of temperature distribution of plasma arc with molten pool in plasma arc melting. Comput Mater Sci 2004;30:441–7.
[9] Liu YJ, Qiao AK, Nan Q, Yang XY, Kim SI, Suh TS. Thermal characteristics of microwave ablation in the vicinity of an arterial bifurcation. In: World congress on medical physics and biomedical engineering 2006. Vol. 14, PTS 1–6. Book series: IFMBE proceedings, vol. 14, Part 1–6; 2007. p. 54–57
[10] Yoon JK. Applications of numerical simulation to continuous casting technology. J Iron Steel Inst Jpn 2008;48(7):879–84.
[11] Zhu J, Kuznetsov AV, Sandeep KP. Investigation of a particulate flow containing spherical particles subjected to microwave heating. Heat Mass Transfer 2008;44:481–93.
[12] Moon FC. Magneto-solid mechanics. J. Wiley & Sons; 1984.
[13] Jin JM. The finite element method in electromagnetics. J. Wiley; 1993.
[14] Jiang BN, Wu J, Povinelli LA. The origin of spurious solutions in computational electromagnetics. J Comput Phys 1996;125:104–23.
[15] Nedelec JC. Mixed finite elements in R3. Numer Math 1980;35:315–41.
[16] Nicomedes WL, Mesquita RC, Moreira FJS. The meshless local Petrov–Galerkin method in two-dimensional electromagnetic wave analysis. IEEE Trans Antennas Propag 2012;60:1957–68.
[17] Badia S, Codina R. A combined nodal continuous-discontinuous finite element formulation for the Maxwell problem. Appl Math Comput 2011;218:4276–94.
[18] Bathe KJ. Advances in the multiphysics analysis of structures. In: Topping BHV, editor. Chapter 1 in computational methods for engineering science. Stirlingshire, Scotland: Saxe-Coburg Publications; 2012.
[19] Bathe KJ, Zhang H. A flow-condition-based interpolation finite element procedure for incompressible fluid flows. Comput Struct 2002;80:1267–77.
[20] Bathe KJ, Zhang H. Finite element developments for general fluid flows with structural interactions. Int J Numer Methods Eng 2004;60:213–32.
[21] Bathe KJ, Zhang H. A mesh adaptivity procedure for CFD and fluid-structure interactions. Comput Struct 2009;87:604–17.
[22] ADINA theory and modeling guides, ADINA R&D Inc., Watertown, MA 02472; http://www.adina.com, 2012.
[23] Bathe KJ. Finite element procedures. Prentice Hall; 1996.
[24] Balanis CA. Advanced engineering electromagnetics. J. Wiley & Sons; 1989.
[25] Bathe KJ, Ledezma GA. Benchmark problems for incompressible fluid flows with structural interactions. Comput Struct 2007;85:628–44.
[26] Timoshenko SP, Gere JM. Theory of elastic stability. McGraw-Hill, 1961.
[27] Weiss J, Csendes ZJ. A one-step finite element method for multiconductor skin effect problems. IEEE Trans Power Appar Syst 1982;PAS-101(10).
[28] Oskooi A, Johnson SG. Electromagnetic wave source conditions. In: Taflove A, Oskooi A, Johnson SG, editors. Chapter 4 in advances in FDTD computational electrodynamics: photonics and nanotechnology. MA, Artech House: Norwood; 2013.
[29] Mur G. Absorbing boundary conditions for the finite-difference approximation of the time-domain electromagnetic-field equations. IEEE Trans Electromagn Compat 1981;EMC-23(4):377–82.